Journal of Materials Chemistry A

PAPER

View Article Online
View Journal | View Issue

Cite this: J. Mater. Chem. A, 2017, 5, 7184

Tuning the selectivity and activity of Au catalysts for carbon dioxide electroreduction *via* grain boundary engineering: a DFT study†

Cunku Dong,[ab] Jianyu Fu,[a] Hui Liu,[a] Tao Ling,[a] Jing Yang,[a] Shi Zhang Qiao *[ac] and Xi-Wen Du *[a]

Received 13th December 2016
Accepted 13th March 2017

DOI: 10.1039/c6ta10733h

rsc.li/materials-a

Au catalysts possess a high activity to yield gaseous carbon monoxide (CO) at moderate overpotentials for the carbon dioxide CO_2 electrochemical reduction reaction (CO_2RR). However, tuning selectivity remains a massive challenge towards the production of hydrocarbon species at relatively low potentials. In this study, by means of first principles calculations we propose a promising strategy to tune the selectivity and activity of Au catalysts *via* grain boundary (GB) engineering. The GB sites on the Au(110) surface are identified to strongly bind *CO so as to compensate for the unsaturated coordination of GB atoms, leading to a high selectivity toward CH_3OH; its catalytic performance is comparable to Cu for generating CH_4. In addition, GBs on the Au(100) surface are also investigated for comparison, which can greatly promote CO production. Our findings suggest that GB engineering is an effective means to improve the CO_2RR performance of a given catalyst, which will motivate reasonable design and synthesis of novel electrocatalysts for CO_2 reduction to produce hydrocarbon species.

1. Introduction

The heterogeneous electrocatalytic CO_2 reduction reaction (CO_2RR) is a promising technique to remedy the environmental and social issues stemming from the emission of greenhouse gases. However, further development of such a technique is restricted by the activity and selectivity of catalysts themselves. Nowadays, a large number of strategies have been proposed to enhance the performance of CO_2RR catalysts by controlling their structure and morphology to expose specific active sites (facets, edges, and corners).[1–4] Although the activity of CO_2RR catalysts is dramatically improved through these strategies, the selectivity (reaction pathway) of a given catalyst cannot be tuned remarkably to yield hydrocarbon species such as CH_4 and CH_3OH.[5–7] Au, Ag and Zn favour the production of CO at moderate overpotentials in aqueous media, whereas Sn, Pb and Bi preferably yield HCOOH.[8,9] These catalysts suffer from further reduction of CO_2 to high-value hydrocarbon products such as CH_3OH or C_2H_5OH. Cu is found to be uniquely able to reduce CO_2 into various hydrocarbon products, but a much higher overpotential is required, especially for high-value liquid fuels (CH_3OH and C_2H_5OH).[10,11] Various methods such as alloying have been proposed, but high selectivity towards hydrocarbon products at low overpotentials is by far not yet achieved.[12,13] Therefore, it remains an enormous challenge to find CO_2RR catalysts for producing hydrocarbon species at moderate overpotentials.

In fact, the selectivity of a given catalyst is ascribed to its ability to bind key intermediate species.[14] For instance, adsorbed CO (*CO) is bound to the Au surface weakly enough to easily desorb off the surface, inhibiting its further protonation.[15] Grain boundary (GB) engineering may offer a promising and feasible means to address this issue. GBs, rich in atomic disorder and microstrain, are believed to facilitate lowering of the activation barrier; thus, the catalytic activity is enhanced in different kinds of reactions.[16–19] Kanan *et al.* reported that GBs on the catalyst surface derived from oxide reduction or e-beam deposition can significantly improve the catalytic activity of the CO_2RR.[20–23] Kim *et al.* theoretically elucidated the mechanism of electrochemical CO_2 reduction at GBs on the Au(111) surface.[24] It is determined that the broken local spatial symmetry near a GB increases the Au metal-to-ligand π-backbonding strength, leading to effective stabilization of the COOH intermediate and thus enhances the CO_2 reduction activity. Unfortunately, the GBs on Au(111) are just prone to enhancing CO production rather than producing more reduced hydrocarbon species. To date, no experimental and theoretical evidence unravels or predicts the possibility of tuning CO_2RR selectivity *via* GBs

[a]Institute of New Energy Materials, School of Materials Science and Engineering, Tianjin University, Tianjin 300072, People's Republic of China. E-mail: xwdu@tju.edu.cn; s.qiao@adelaide.edu.au

[b]Key Laboratory of Advanced Ceramics and Machining Technology, Ministry of Education, Tianjin University, Tianjin, 300072, People's Republic of China

[c]School of Chemical Engineering, University of Adelaide, Adelaide, SA 5005, Australia

† Electronic supplementary information (ESI) available: Computational details and free-energy correction terms for free gas and adsorbates are summarized. Free energy diagrams for the CO_2RR at $U = 0$ V on sites 1–4 on Au(100) GBS and Au(100) GBS are presented. See DOI: 10.1039/c6ta10733h

toward protonating adsorbed *CO for originally inactive metal catalysts.

Inspired by GBs featuring a disorder in the atomic arrangement or broken local spatial symmetry,[24] which probably alters the local electronic structure, we systematically investigate the catalytic properties of GBs on Au catalysts by means of first principles calculations. The Au(110) plane is an active low-index facet for the CO_2RR, which is experimentally obtained[25–27] and observed *via* atomic resolution transmission electron microscopy.[28,29] Accordingly, we focus on the role of GBs on the Au(110) surface in tuning selectivity towards hydrocarbon products. In contrast with Au(111), we find that active sites at GBs on Au(110) efficiently tune the electroreduction pathway of CO_2 to produce the liquid product CH_3OH by enhancing the *CO binding capability, which is comparable to Cu(211) in the catalytic performance to generate CH_4. From this point of view, GB engineering is a promising means to alter the reaction pathway of the CO_2RR for other originally inactive catalysts to produce hydrocarbon species, and aid the rational design of more selective CO_2RR catalysts *via* creating grain boundaries at a specific facet.

2. Models and methods

Two GB bulk models with low-index (100) and (110) facets were built according to the coincidence site lattice (CSL) theory,[30,31] denoted as Au$\sum$5{021}/[100] GB and Au$\sum$6{2-21}/[110] GB, as displayed in Fig. 1 (see ESI† for details). A low-index AuGB surface (GBS) was constructed *via* exposing the corresponding low-index planes such as the (100) and (110) planes, denoted as Au(100) GBS and Au(110) GBS, respectively.

All periodic density functional theory (DFT) calculations in this study were performed using the Vienna ab initio simulation program (VASP), a plane-wave DFT software package.[32] The exchange–correlation interactions were modeled using a revised Perdew–Burke–Ernzerhof (rPBE) functional within the generalized gradient approximation (GGA) implemented with the projector-augmented-wave (PAW) function method for representing the nonvalence core electrons. Spin-polarization was considered in all calculations except for free gaseous species. A plane-wave cutoff energy was set as 450 eV. 0.1 eV of Fermi-level smearing was used for all geometrical relaxation, including bulk, adsorbate-surface and gas-phase species. The relaxation for these systems was completed when the maximum force exerted on each atom is less than 0.05 eV $Å^{-1}$. The adsorption of intermediates at the atop sites is considered for various catalysts. The perfect Au bulk was fully optimized using 16 × 16 × 16 *k*-point Monkhorst–Pack mesh sampling. For Au slab calculations, 2 × 1 × 1 *k*-point Monkhorst–Pack mesh sampling was employed for the AuGBS and GB-free surface in the surface Brillouin zone.

3. Results and discussion

The grain boundary is built according to the CSL theory, where Au atoms are in closer proximity in the vicinity of GBs. However, this proximity will lead to an unstable GB structure with increased coulombic repulsion and high GB energy. To lower GB energy and obtain stable GBs, vacancies were introduced along the GBs so as to reduce the atomic density,[33,34] as proposed by Yoshiya *et al.*[35] After the full relaxation, the configuration is reconstructed to obtain the stable GB structure for the adsorption simulations (Fig. 1).

Four active sites were chosen for each Au GB surface (AuGBS) to compare the catalytic activity (see inset in Fig. 2). Sites 1–3 are GB sites while site 4 is the neighboring site. An approximate

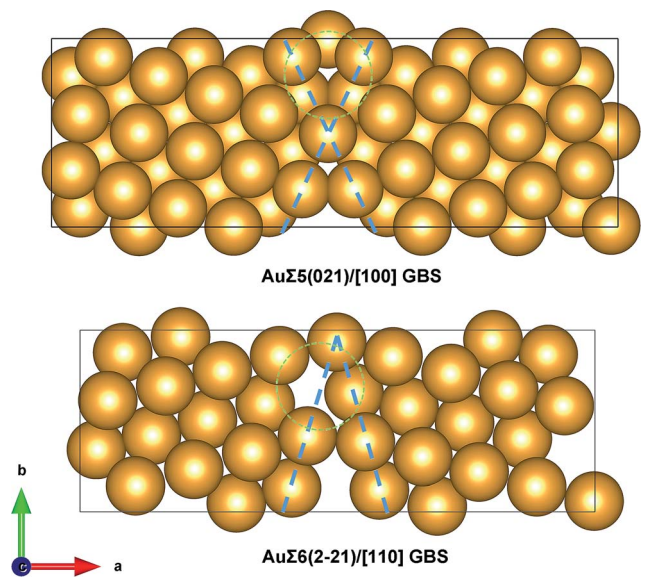

Fig. 1 Top view of a periodic supercell for initial built-up low-index AuGBS, Au$\sum$5(021)/[100] GBS and Au$\sum$6(2-21)/[110] GBS, respectively. The black line indicates the boundary of a unit supercell. The GBS area is enclosed by the blue dashed lines and the vacancy is marked by the green dashed circles.

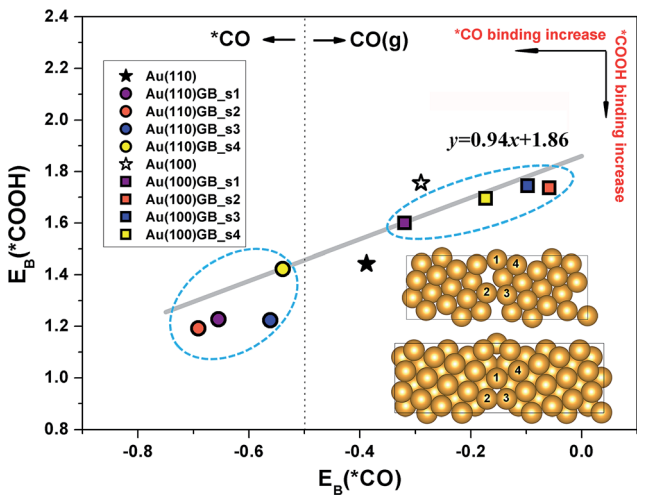

Fig. 2 Adsorption energy scaling relationship between E_B[*COOH] and E_B[*CO] for various sites on AuGBS and the flat Au surface. Au(110)_s1, for example, represents site 1 on Au(110) GBS. The vertical dashed line indicates a threshold E_B[*CO]: on the right of this line gaseous CO is preferably released, whereas on the left adsorbed *CO on the catalyst is favourable.

scaling relationship between E_B[*COOH] and E_B[*CO] is clearly observed, quite consistent with the previous study.[15] We also find a facet- and site-dependent sensitivity towards stabilizing *COOH. For Au(100) GBS, site 1 binds *COOH most strongly in comparison with flat Au(100) with an E_B[*COOH] of 1.60 eV. Nevertheless, other sites at and in the vicinity of the GB (sites 2–4) have a slightly weaker ability to bind *COOH than flat Au(100). In contrast, for Au(110) GBS sites except site 4 can greatly stabilize *COOH. In particular, site 2 binds *COOH most strongly with an E_B[*COOH] of 1.19 eV, which is 0.25 eV lower than that of flat Au(110) (E_B[*COOH] = 1.44 eV). Therefore, GBs have a positive impact on the activation of CO_2 to form stable *COOH.

The *CO binding ability of AuGBS and flat Au is also presented in Fig. 2, as a descriptor to estimate the capability to further protonate *CO (E_B[*CO]). A distinct difference in the *CO binding trend is noted for Au(100) GBS and Au(110) GBS, exhibiting a facet-sensitive behaviour. To be more specific, GBs on Au(100) would readily liberate CO due to the oppressed E_B[*CO], which is less than the optimal CO binding energy (−0.5 eV). In this case, CO will be released in an ultrafast manner once *CO is generated on Au(100) GBS. In contrast, *CO is markedly stabilized on Au(110) GBS (E_B[*CO] > −0.5 eV); that is, *CO is thermodynamically favoured on Au(110) GBS. Consequently, further protonation of *CO is expected to occur on Au(110) GBS. More importantly, the neighbouring site 4 is activated to bind *CO strongly, akin to the GB sites (sites 1–3). As such, the existing GBs not only improve the catalytic property on their own, but also activate other sites nearby.

Free energy profiles are presented to explore the feasibility of the formation of the key intermediate *COOH (Fig. 3A). Considering inconsistency between theoretical and experimental gas-phase reaction enthalpies, a correction of +0.45 eV is added for gaseous CO_2 to the electronic energy.[36] Besides, 0.25 and 0.5 eV stabilization are applied for COOH* and *OH, respectively, for all surfaces, owing to the solvation effect in aqueous solutions.[37–40] For *CO and *CHO, the stabilization was approximately calculated to be −0.1 eV.[36] Obviously, GBs on Au surfaces can significantly reduce the reaction barrier of CO_2 → *COOH with respect to the flat Au surface. For Au(100) GBS, a significant uphill process is followed by two sequential downhills, indicating that CO release is exergonic (downhill in energy). Therefore, Au(100) GBS cannot change the reaction pathway, but just lower the overpotential for producing gaseous CO. According to the free energy profile, the Au(110) is determined to be the most active for forming *COOH and binding *CO among common low-index facets such as Au(100), Au(111) and Au(110).[15] We notice an obvious uphill with a substantial energy cost (0.28 eV) in the process of *CO → CO(g) for Au(110) GBS; thus, *CO will be immediately stably bound to GBs sites once formed, a prerequisite for further reduction of *CO. More importantly, Au(110) GBS allows ΔG(*CO) significantly to drop to −0.17 eV, superior to conventional Cu(211). Additionally, active sites (sites 1–4) on Au(110) GBS feature a lower ΔG(CO_2 → *COOH) compared with Cu(211).

The hydrogen evolution reaction (HER) impedes the desired reaction for the CO_2RR as a dominant competing reaction.[41] In

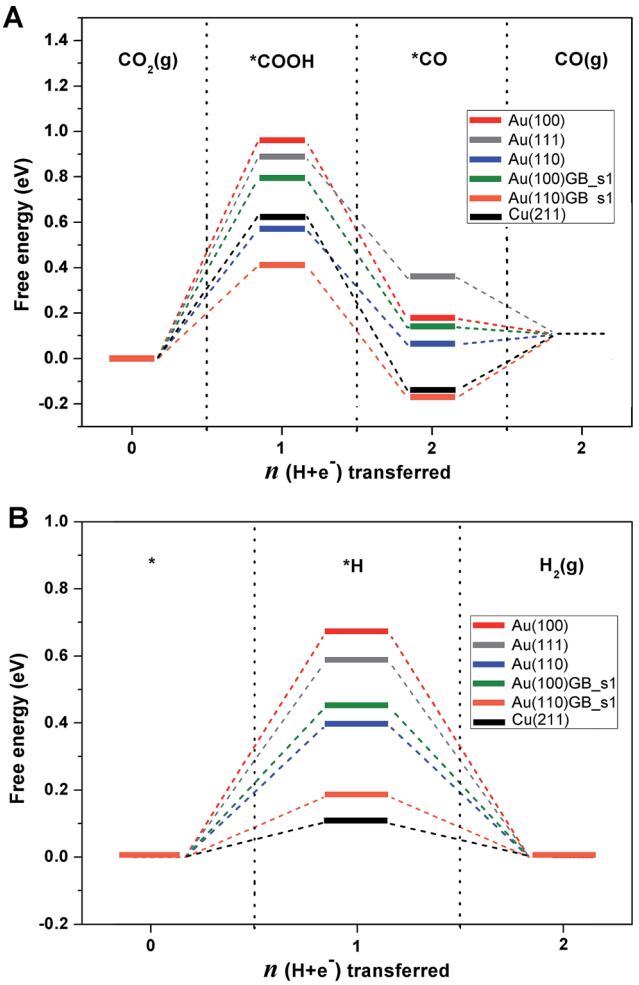

Fig. 3 Free energy diagrams for (A) CO_2RR and (B) HER at zero electrode potential (U = 0 V) at site 1 on AuGBS and the flat Au surface. n indicates the number of proton–electron pairs transferred during the CO_2RR and HER. The asterisk alone represents a clean surface, while *COOH, for example, means the COOH intermediate binding to the surface.

Fig. 3B, we present ΔG(*H) for the HER occurring at site 1 on Au(100) GBS and Au(110) GBS. Obviously, the overpotential for the HER is lowered in the same manner as for the CO_2RR through strongly binding *H. Nevertheless, we cannot arbitrarily conclude that AuGBS is not a good candidate for reducing CO_2, as the CO_2RR and HER jointly determine the selectivity in the process of CO_2 electroreduction. The difference in U_L between the CO_2RR and HER, $U_L(CO_2) - U_L(H_2)$, is an accurate descriptor to identify the trend in selectivity toward carbonaceous products for CO_2RR catalysts.[42,43] The higher $[U_L(CO_2) - U_L(H_2)]$ implies the higher selectivity for the CO_2RR over the HER. Table 1 summarizes $[U_L(CO_2) - U_L(H_2)]$ of site 1 on AuGBS and the flat Au surface. We find that this difference for site 1 on AuGBS is rather close to that for the flat Au surface. This illustrates that the GBS has a similar selectivity toward carbon-based products as a GBS-free Au catalyst.

We predict the activity and selectivity by the elementary U_L volcano plot (Fig. 4). The theoretical overpotential (η) required

Table 1 Limiting potentials for the CO_2RR and HER and $U_L(CO_2) - U_L(H_2)$ for as-selected site 1 on AuGBS and the flat Au surface[a]

	$U_L(CO_2)$ (V)	$U_L(H_2)$ (V)	$U_L(CO_2) - U_L(H_2)$ (V)
Au(100)	−1.21	−0.66	−0.55
Au(110)	−0.82	−0.39	−0.43
Au(100) GBS_site 1	−1.05	−0.44	−0.51
Au(110) GBS_site 1	−0.65	−0.18	−0.47

[a] $U_L(CO_2)$ is calculated from the pathway to yield CO(g).

for each elementary step is estimated by the difference between each U_L and the equilibrium potential (U_{eq}), $\eta = U_L - U_{eq}$. At more negative potentials than U_L, the elementary step becomes exergonic and proceeds at an appreciable rate. PDS is thus determined by the most negative U_L lines. In Fig. 4A, two downmost U_L lines correspond to PDSs for various catalysts, representing $CO_2(g) \rightarrow$ *COOH and *CO → *CHO transformation, respectively. Obviously, the formation of *COOH on Au and Ag is generally the PDS for the overall CO_2RR, whereas Cu and Ni have to overcome the barrier of *CO → *CHO.

We note that Au(100) GBS is located at the U_L line of $CO_2(g) \rightarrow$ *COOH, to the right of the volcano top, indicating that $CO_2(g) \rightarrow$ *COOH is still the PDS similar to the flat Au (Fig. 4A). Besides, *CO is favourably released on Au(100) GBS because of the binding energy much smaller than the threshold E_B[*CO] = −0.5 eV. Thus, Au(100) GBS cannot radically change the CO_2 electroreduction pathway but facilitates CO release. In contrast, the sites on Au(110) GBS have a large E_B(*CO) ranging from −0.54 to −0.69 eV, close to the −0.65 eV of Cu(211) at the U_L line of *CO → *CHO near the top of the "volcano"-type relation.[44] The protonation of *CO to form *CHO is thus the PDS rather than $CO_2(g) \rightarrow$ *COOH owing to the strong ability of Au(110) GBS to bind *CO, a prerequisite for the subsequent protonation of *CO. Therefore, the overall electrocatalytic pathway for Au(110) GBS can be altered by facilitating the formation of *CHO (Fig. 4C).

For the selectivity estimation, only C1 hydrocarbon products are considered (*i.e.* CH_3OH and CH_4) in our work. We present the plot of U_L as a function of E_B[OH] for various catalysts in two important reaction steps (*$OCH_3 \rightarrow CH_3OH$ and *$OCH_3 \rightarrow$ *O + CH_4), as illustrated in Fig. 4B. A typical volcano behaviour is also observed for these elementary steps that involve

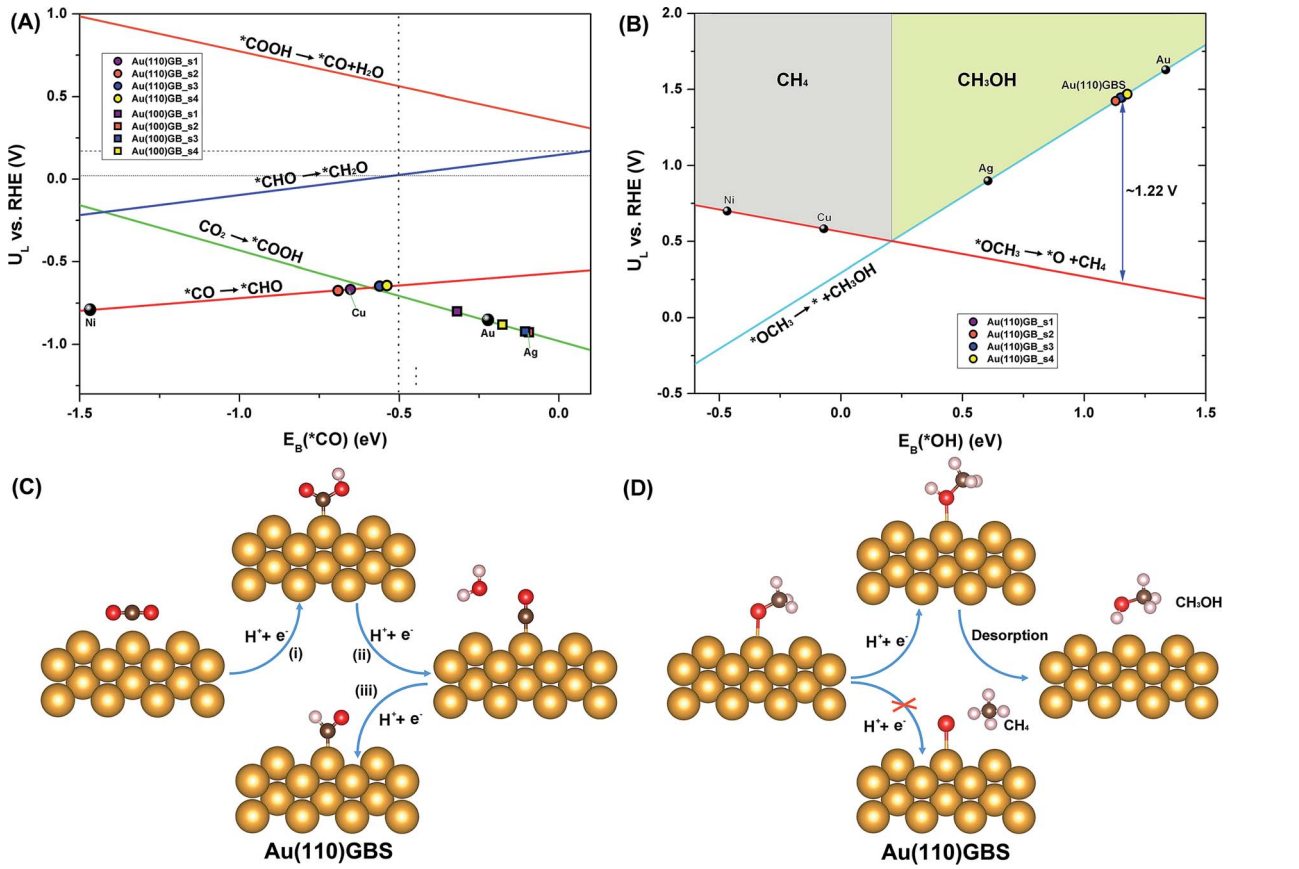

Fig. 4 Predicted limiting potentials (U_L) for elementary proton-transfer steps as a function of the intermediate binding affinity through (A) carbon and (B) oxygen, *i.e.* E_B[CO] or E_B[OH]. Schematic illustration of the protonation of CO_2 to yield *CHO (C) and OCH_3 to CH_3OH (D) on Au(110) GBS, respectively. In (A) and (B), each line represents an elementary reaction, which is plotted by using the scaling relation principle. The equilibrium potentials for the overall electrochemical reduction of CO_2 to CH_4 and CH_3OH are +0.17 and +0.02 V *versus* the RHE which are indicated by horizontal dashed lines, respectively. The vertical dashed line represents the threshold E_B[*CO] between adsorbed *CO on the catalysts and released CO(g). The favourable production of CH_4 and CH_3OH is highlighted in grey and yellow, respectively.

intermediates binding through oxygen. The selectivity of either CH_3OH or CH_4 is determined by the binding ability of the oxygen bond. That is, a weak binding strength for (*)-OCH_3 preferentially leads to the generation of CH_3OH *via* the desorption of the whole *OCH_3 group from the catalyst surface, while a strong binding ability for *O–CH_3 is apt to yield CH_4 as a dominant product through breaking of the O–CH_3 bond.[45] Two possible U_L lines for the elementary steps determine the selectivity of CH_3OH or CH_4. In the light of strong *CO binding ability, only Au(110) GBS is considered for selectivity evaluation. Au(110) GBS is situated on the right-side of the OH-analogous volcano plot and far from the top. In addition, Au(110) GBS has a thermodynamic preference for CH_3OH over CH_4 by ~1.22 eV. These results indicate that Au(110) GBS favours the production of liquid fuel CH_3OH rather than gaseous CH_4 (Fig. 4D). By comparison, CH_4 production is preferred on the Cu catalyst as a major product over CH_3OH.[45,46]

In order to further evaluate the activity and selectivity of Au(110) GBS to reduce *CO to hydrocarbon species, we compare the full CO_2RR pathway of the Au(110) GBS and conventional Cu(211) flat surface. Fig. 5 shows the free energy diagram for the reduction of CO_2 to CH_4 or CH_3OH (shown in orange). Obviously, Au(110) GBS and Cu(211) have a similar overall CO_2RR pathway from CO_2 to *CHO. Two key energy barriers along the overall CO_2RR pathway are observed, corresponding to two PDSs, *i.e.* CO_2 → *COOH and *CO → *CHO, which are in good agreement with previous theoretical studies.[44] Thereinto, site 1 on Au(110) GBS has an energy barrier of 0.41 eV for CO_2 → *COOH transformation, which is 0.21 eV lower than that of Cu(211).

Along the overall CO_2RR pathway, the PDS for Au(110) GBS and Cu (211) is *CO → *CHO instead of CO_2 → *COOH. The calculated U_L of this PDS for site 1 (−0.64 V) is smaller than that for Cu (−0.73 V), indicating that GBs not only alter the CO_2RR pathway, but also lower the overpotential required for further reduction. The U_L of −0.73 V in this study is in good agreement with the previous result (−0.74 V).[36] As a result, Au(110) GBS outperforms the current Cu electrode in the overall energy cost. As stated above, this step occurs owing to the relatively strong ability of Au(110) GBS to bind *CO, which leads to two phenomena: (i) in lower potential ranges, *CO can desorb off the Au(110) GBS surface to produce CO(g) by just overcoming the *CO → CO(g) barrier; (ii) when an external potential more than U_L = −0.64 eV is applied, the *CO → *CHO step is immediately activated to protonate *CO thermodynamically, yielding more reduced species such as CH_3OH.

For Cu(211), two proton–electron pair transfer steps are thermodynamically spontaneous in the process of *CHO → *CH_3O, as presented by two successive downhills. Nevertheless, these two protonation processes are exergonic (uphill in free energy) for Au(110) GBS. The sixth proton–electron pair transfer step is the selectivity-determining step (Fig. 5), which determines the final product (CH_4 or CH_3OH). The thermodynamic preference for CH_3OH over CH_4 is much larger for the Au(110) GBS site 1 (1.11 eV) than for Cu(211) (0.37 eV). This result indicates that Au(110) GBS is prone to producing CH_3OH rather than CH_4. The desired final product varies as a result of *OH binding strength (E_B[OH]) as a suitable selectivity-determining descriptor,[46] as proven above. We use the Arrhenius formula $k = A\exp[-(\Delta G)/(RT)]$ to estimate the product distribution for Au(110) GBS based on the thermodynamic free energy difference ($\Delta G = G_{CH_3OH} - G_{*O+CH_4}$). By substituting ΔG with −1.11 eV and T with 298.15 K, the CH_3OH : CH_4 molar ratio is calculated to be ~exp (43) : 1 at ambient temperature. Au(110) GBS has an extremely high selectivity toward CH_3OH. The feasibility of further reduction of *CO to CH_3OH at site 2 is also shown in Fig. 5. This site behaves similarly to site 1 for selectively producing CH_3OH. Therefore, Au(110) GBS is indeed comparable to Cu in further protonating *CO, although the final product is different.

To unravel the origin of the potential of GBs to tune the CO_2RR pathway and activity, we used the concept of "generalized" coordination numbers ($\overline{CN}$) as an approximate descriptor

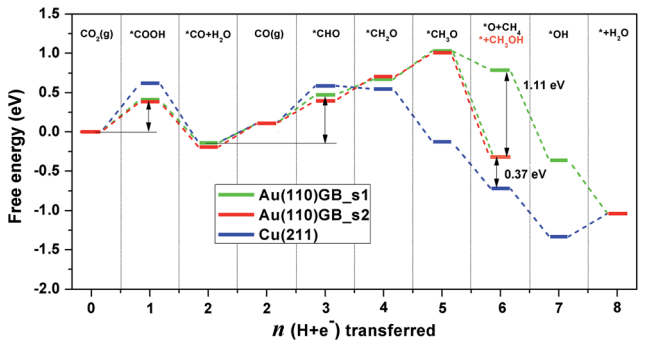

Fig. 5 Free energy diagrams of the overall CO_2RR pathway for sites 1 and 2 on Au(110) GBS and Cu(211) at 0 V *vs.* the RHE. The (*+CH_3OH) state is marked in orange. *n* indicates the number of proton–electron pairs transferred during the CO_2RR.

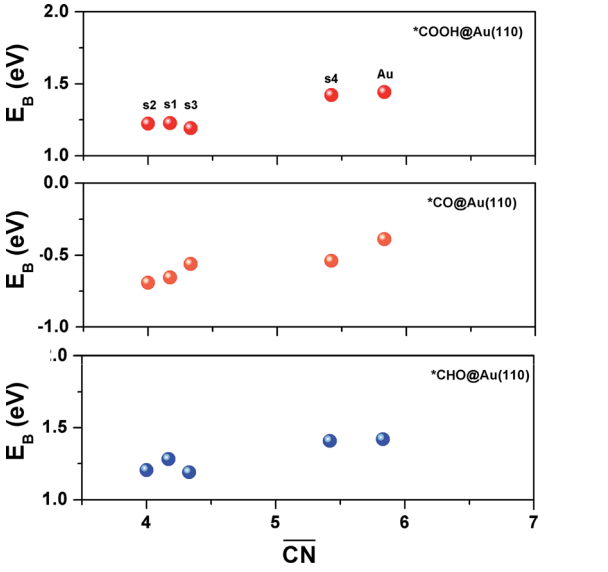

Fig. 6 Trends in the binding energy of *COOH, *CO and *CHO in the PDSs taking placing on Au(110) GBS and the flat Au(100) surface as a function of $\overline{CN}$. s1–4 represent sites 1–4 on Au(110) GBS, whereas Au means the flat Au(100) surface.

from the geometrical point of view. $\overline{CN}$ can identify the trend in adsorption energies for small species by using the geometrical structure of active sites, which has been used to successfully predict the optimal active sites for the oxygen reduction reaction (ORR) of the Pt catalyst.[47,48] In our study, this concept is appropriate to describe the impact of GBs on catalytic properties because GBs are rich in the disorder of the atomic arrangement. In Fig. 6, we notice a $\overline{CN}$-dependent activity for binding key intermediates in the PDSs such as *COOH, *CO and *CHO on Au(110) GBS. Generally, a smaller $\overline{CN}$ corresponds to the atom having a larger binding energy (E_B) for these key intermediates formed in the process of CO_2 protonation. Hence, a smaller $\overline{CN}$ favours the further protonation of *CO to produce CH_3OH on Au(110) GBS, and *CHO is readily stabilized. $\overline{CN}$ can outline the geometric structure of optimal active sites. The difference in the binding energy between AuGBS and the flat surface is due to the lack of coordination of surface atoms at and near GBs, where the crystal lattice loses the periodic and systematic arrangement. This disorder is linked to their response towards the formation of new bonds that compensate for the lack of coordination,[49,50] following the bond-order conservation theory.[51,52]

4. Conclusions

In summary, GBs on Au surfaces are rich in the disorder of the atomic arrangement, and thus active sites around GBs lose the complete coordination, which leads to the formation of strong bonds between intermediates and Au surfaces that compensate for the lack of coordination. GBs on Au(110) tune the electroreaction pathway of CO_2 to selectively produce liquid CH_3OH by significantly stabilizing *CO, which is comparable to Cu(211) in the catalytic performance to generate CH_4. In addition, GBs on the Au(100) surface are also investigated for comparison, which can greatly promote CO production. This work is likely to spark further investigation into GB effects that will contribute to the deep understanding of controlling selectivity, and aid the design of more selective CO_2RR catalysts *via* creating grain boundaries at a specific facet for allowing originally inactive catalysts to be activated to produce high value-added fuels.

Acknowledgements

This research was supported by the National Key Basic Research Program of China (2014CB931703), National Natural Science Foundation of China (21403152, 51471115 and 51171127, 51671141, 21576202), and Tianjin Natural Science Foundation (16JCQNJC05700).

Notes and references

1 H. Mistry, R. Reske, Z. Zeng, Z.-J. Zhao, J. Greeley, P. Strasser and B. R. Cuenya, *J. Am. Chem. Soc.*, 2014, **136**, 16473–16476.
2 D. Gao, H. Zhou, J. Wang, S. Miao, F. Yang, G. Wang, J. Wang and X. Bao, *J. Am. Chem. Soc.*, 2015, **137**, 4288–4291.
3 M. Ma, K. Djanashvili and W. A. Smith, *Angew. Chem., Int. Ed.*, 2016, **55**, 6680–6684.
4 Q. Lu, J. Rosen, Y. Zhou, G. S. Hutchings, Y. C. Kimmel, J. G. Chen and F. Jiao, *Nat. Commun.*, 2014, **5**, 3242.
5 R. J. Lim, M. Xie, M. A. Sk, J.-M. Lee, A. Fisher, X. Wang and K. H. Lim, *Catal. Today*, 2014, **233**, 169–180.
6 Z.-L. Wang, C. Li and Y. Yamauchi, *Nano Today*, 2016, **11**, 373–391.
7 J. Albo, M. Alvarez-Guerra, P. Castaño and A. Irabien, *Green Chem.*, 2015, **17**, 2304–2324.
8 Y. Hori, in *Modern Aspects of Electrochemistry*, 2008, vol. 42, pp. 89–189.
9 D. D. Zhu, J. L. Liu and S. Z. Qiao, *Adv. Mater.*, 2016, **28**, 3423–3452.
10 Y. Hori, A. Murata and R. Takahashi, *J. Chem. Soc., Faraday Trans. 1*, 1989, **85**, 2309–2326.
11 K. J. P. Schouten, E. Perez Gallent and M. T. M. Koper, *ACS Catal.*, 2013, **3**, 1292–1295.
12 D. A. Torelli, S. A. Francis, J. C. Crompton, A. Javier, J. R. Thompson, B. S. Brunschwig, M. P. Soriaga and N. S. Lewis, *ACS Catal.*, 2016, **6**, 2100–2104.
13 D. Ren, B. S. Ang and B. S. Yeo, *ACS Catal.*, 2016, **6**, 8239–8247.
14 Y. Li and Q. Sun, *Adv. Energy Mater.*, 2016, **6**, 1600463.
15 S. Back, M. S. Yeom and Y. Jung, *ACS Catal.*, 2015, **5**, 5089–5096.
16 R. Vidruk, M. V. Landau, M. Herskowitz, M. Talianker, N. Frage, V. Ezersky and N. Froumin, *J. Catal.*, 2009, **263**, 196–204.
17 R. Vidruk, M. V. Landau, M. Herskowitz, V. Ezersky and A. Goldbourt, *J. Catal.*, 2011, **282**, 215–227.
18 A. N. Gavrilov, E. R. Savinova, P. A. Simonov, V. I. Zaikovskii, S. V. Cherepanova, G. A. Tsirlina and V. N. Parmon, *Phys. Chem. Chem. Phys.*, 2007, **9**, 5476–5489.
19 C. W. Li, J. Ciston and M. W. Kanan, *Nature*, 2014, **508**, 504–507.
20 X. Feng, K. Jiang, S. Fan and M. W. Kanan, *J. Am. Chem. Soc.*, 2015, **137**, 4606–4609.
21 X. Feng, K. Jiang, S. Fan and M. W. Kanan, *ACS Cent. Sci.*, 2016, **2**, 169–174.
22 A. Verdaguer-Casadevall, C. W. Li, T. P. Johansson, S. B. Scott, J. T. McKeown, M. Kumar, I. E. L. Stephens, M. W. Kanan and I. Chorkendorff, *J. Am. Chem. Soc.*, 2015, **137**, 9808–9811.
23 C. W. Li and M. W. Kanan, *J. Am. Chem. Soc.*, 2012, **134**, 7231–7234.
24 K.-S. Kim, W. J. Kim, H.-K. Lim, E. K. Lee and H. Kim, *ACS Catal.*, 2016, **6**, 4443–4448.
25 N. Hauptmann, R. Robles, P. Abufager, N. Lorente and R. Berndt, *J. Phys. Chem. Lett.*, 2016, **7**, 1984–1990.
26 S. Fortuna, P. Gargiani, M. G. Betti, C. Mariani, A. Calzolari, S. Modesti and S. Fabris, *J. Phys. Chem. C*, 2012, **116**, 6251–6258.
27 S. Nakanishi, G. Lu, H. M. Kothari, E. W. Bohannan and J. A. Switzer, *J. Am. Chem. Soc.*, 2003, **125**, 14998–14999.
28 T. Radetic, F. Lançon and U. Dahmane, *Phys. Rev. Lett.*, 2002, **89**, 085502.
29 T. Radetic and U. Dahmen, Relaxation of grain boundaries in Au{110} mazed bicrystal thin films observed by HREM,

Thin Films: Stresses and Mechanical Properties Ix, ed. C. S. Ozkan, L. B. Freund, B. C. Cammarata and H. Gao, 2002, vol. 695, pp. 47–52.
30 A. P. Sutton and R. W. Balluffi, *Interfaces in Crystalline Materials*, Oxford Scientific Publications, Oxford, 1995.
31 E. W. Hart, *The Nature and Behavior of Grain Boundaries*, Plenum, New York, 1972, p. 155.
32 G. Kresse and D. Joubert, *Phys. Rev. B: Condens. Matter Mater. Phys.*, 1999, **59**, 1758.
33 J. A. Dawson and I. Tanaka, *J. Mater. Chem. A*, 2014, **2**, 1400–1408.
34 J. A. Dawson, H. Chen and I. Tanaka, *ACS Appl. Mater. Interfaces*, 2015, **7**, 1726–1734.
35 M. Yoshiya and T. Oyama, *J. Mater. Sci.*, 2011, **46**, 4176–4190.
36 A. A. Peterson, F. Abild-Pedersen, F. Studt, J. Rossmeisl and J. K. Nørskov, *Energy Environ. Sci.*, 2010, **3**, 1311–1315.
37 J. K. Nørskov, J. Rossmeisl, A. Logadottir, L. Lindqvist, J. R. Kitchin, T. Bligaard and H. Jonsson, *J. Phys. Chem. B*, 2004, **108**, 17886–17892.
38 J. Rossmeisl, J. Greeley and G. Karlberg, *Electrocatalysis and Catalyst Screening from Density Functional Theory Calculations. Fuel Cell Catalysis: a Surface Science Approach*, Wiley, Hoboken, NJ, ch. 3, 2009, pp. 57–92.
39 G. Karlberg and G. Wahnström, *Phys. Rev. Lett.*, 2004, **92**, 136103.
40 V. Tripković, E. Skúlason, S. Siahrostami, J. K. Nørskov and J. Rossmeisl, *Electrochim. Acta*, 2010, **55**, 7975–7981.
41 R. Zhang, W. Lv and L. Lei, *Appl. Surf. Sci.*, 2015, **356**, 24–29.
42 C. Shi, H. A. Hansen, A. C. Lausche and J. K. Nørskov, *Phys. Chem. Chem. Phys.*, 2014, **16**, 4720–4727.
43 K. Chan, C. Tsai, H. A. Hansen and J. K. Nørskov, *ChemCatChem*, 2014, **6**, 1899–1905.
44 D. Cheng, F. R. Negreiros, E. Aprà and A. Fortunelli, *ChemSusChem*, 2013, **6**, 944–965.
45 S. Back, H. Kim and Y. Jung, *ACS Catal.*, 2015, **5**, 965–971.
46 Y. Hori, in *Modern Aspects of Electrochemistry*, vol. 42, 2008, pp. 89–189.
47 F. Calle-Vallejo, J. Tymoczko, V. Colic, Q. H. Vu, M. D. Pohl, K. Morgenstern, D. Loffreda, P. Sautet, W. Schuhmann and A. S. Bandarenka, *Science*, 2015, **350**, 185–189.
48 F. Calle-Vallejo, J. I. Martínez, J. M. García-Lastra, P. Sautet and D. Loffreda, *Angew. Chem., Int. Ed.*, 2014, **53**, 8316–8319.
49 A. Groß, *J. Comput. Theor. Nanosci.*, 2008, **5**, 894–922.
50 A. Peterson, L. Grabow, T. Brennan, B. Shong, C. Ooi, D. Wu, C. Li, A. Kushwaha, A. Medford, F. Mbuga, L. Li and J. Nørskov, *Top. Catal.*, 2012, **55**, 1276–1282.
51 E. Shustorovich and H. Sellers, *Surf. Sci. Rep.*, 1998, **31**, 1–119.
52 J. Kleis, J. Greeley, N. A. Romero, V. A. Morozov, H. Falsig, A. H. Larsen, J. Lu, J. J. Mortensen, M. Dułak, K. S. Thygesen, J. K. Nørskov and K. W. Jacobsen, *Catal. Lett.*, 2011, **141**, 1067–1071.